Singly differential studies of one-electron processes in He²⁺-He collisions

Sh. U. Alladustov [1,*] C. T. Plowman [1] M. S. Schöffler,[2] I. Bray [1] and A. S. Kadyrov [1,3]

[1]*Department of Physics and Astronomy, Curtin University, GPO Box U1987, Perth, WA 6845, Australia*
[2]*Institut für Kernphysik, Universität Frankfurt, 60438 Frankfurt, Germany*
[3]*Institute of Nuclear Physics, Ulugbek, Tashkent 100214, Uzbekistan*

The differential ³He²⁺-He scattering problem is investigated using the two-center wave-packet convergent close-coupling method in the incident energy range of 50–630 keV/u. The present two-electron approach accounts for electron exchange between reaction fragments and uses the configuration-interaction method to treat the target structure. We also apply a simpler method based on the effective one-electron target description. The singly differential cross sections are presented for electron capture, elastic scattering, excitation, and ionization of the target. The paper demonstrates the importance of the electron-electron correlation at lower projectile energies for the electron-capture and elastic-scattering processes. The two-electron results for electron capture into the ground state describe the available experimental data very well at all projectile energies, while the effective single-electron model shows good consistency at energies starting from 300 keV/u. For ionization, we observe a good level of agreement between the two approaches for all types of singly differential cross sections, and they agree well with the experimental data, wherever available. In addition, the angular differential cross sections for ground-state and total electron capture are presented for ⁴He²⁺-He collisions at the projectile energies of 62.5, 125, 187.5, and 250 keV/u. The angular differential elastic-scattering and excitation cross section and all three types of the singly differential ionization cross sections are found to be practically the same as the corresponding results for ³He²-He collisions.

I. INTRODUCTION

Collisions of fully stripped ions with helium have been the subject of a great number of experimental and theoretical research works. Particularly, the ⁴He²⁺-He scattering problem has attracted considerable attention due to its symmetric nature. One of the experimental challenges of investigating this system is the indistinguishability of the formed and residual ions after the collision. For example, once a target electron is captured by the projectile, both the formed and the residual ions are ⁴He⁺ ions, which complicates the measurements of the electron-capture cross sections. Many experimental [1–7] and theoretical [1,8–11] studies of He²⁺-He collisions focused on providing integrated cross sections for various one- and two-electron collisional processes. However, the singly differential cross sections (SDCSs) were not investigated as extensively as the total cross sections. There are some experimental results available for electron capture into the ground state [12–14], which were obtained using the cold target recoil ion momentum spectroscopy technique, and for the singly differential cross section as a function of ejected-electron angle measured using an electron spectrometer [15]. Atomic collisional data for neutral beam modeling in fusion plasmas have recently been reviewed by Hill *et al.* [16].

A number of theoretical approaches were applied to calculate the angular differential cross section for electron capture

into the ground state. Zapukhlyak and Kirchner [17] employed the two-center basis generator method (TC-BGM) based on the independent-electron model (IEM). In the approach, the time-dependent Schrödinger operator, where the Hamiltonian is of a single-particle form with an effective ground-state potential, is solved by the TC-BGM. In the IEM the final two-electron states are described by the symmetrized products of single-particle states. The TC-BGM results demonstrated very good agreement with the available experiments not only for single-electron capture, but also for two-electron processes including double-electron capture and transfer excitation.

Several forms of the continuum distorted-wave (CDW) approach were also applied to study the differential electron-capture cross sections in He²⁺-He collisions. The Born initial-state (BIS) approximation method [14] was employed within the CDW approach, where an asymmetrical model of the entrance and exit channels is used to describe the captured electron. The exit channel wave function was described by the four-body CDW method, and for the entrance channel the four-body first Born approximation (FBA) was used. The approach produced a differential picture of the process with some unphysical dips not compatible with the experiment, but it described the experiment well at small scattering angles for most of the projectile energies considered.

Velayati *et al.* [18] applied the CDW approach using the eikonal initial-state (EIS) and eikonal final-state (EFS) descriptions. In the EIS approach, the initial state is described by the eikonal wave function and the final state is described by the distorted wave. In the EFS implementation, it was the

*sh.alladustov@gmail.com

opposite. The independent-particle model was employed in both approaches. The methods agreed with each other reasonably well, but there were some noticeable deviations at the lowest collision energy considered.

Apart from the CDW approaches, Velayati *et al.* [18] applied the classical trajectory Monte Carlo (CTMC) method. The authors concluded that their theoretical approaches can describe the experiment at some projectile energies at particular scattering angles, but in general none were able to provide a consistent differential description of the charge-transfer dynamics of ^{3}He^{2+}-He collisions.

The three-body (3B) and four-body (4B) Coulomb-Born distorted-wave (CBDW) approximations were applied by Ghanbari-Adivi and Ghavaminia in Refs. [19] and [20], respectively. Post and prior forms of the transition amplitude were calculated in both approaches. It was found that the three-body model was in reasonable agreement with the experiment and other theories, however the four-body results were not in satisfactory agreement with the experimental data. The CBDW-4B results described the experiment reasonably well at small scattering angles. However, as the scattering angle is increased, the results exhibited unphysical dips.

Single-electron capture and transfer-excitation processes in He^{2+}-He collisions were also investigated by Jana and Purkait [21] using the CBDW-4B approach and another method based on the four-body boundary-corrected continuum-intermediate-state (BCCIS-4B) approximation. For electron capture, both the CBDW-4B and BCCIS-4B results considerably overestimated the experimental data in the entire scattering angle range where the data are available, at all considered collision energies. For transfer excitation, the two results were in reasonable agreement with each other and the experiment. Later, Jana *et al.* [22] applied another version of the distorted-wave approximation within the four-body formalism (DW-4B) with some improvements. In particular, the wave functions of all channels were chosen to satisfy the correct boundary conditions, a shorter-range interaction potential was used, and the electron-electron correlation effects were taken into account. Agreement between the DW-4B results and the experiment was very good. Samaddar *et al.* [23] also addressed the same scattering problem using the four-body formalism of the target continuum-distorted-wave approximation, where the independent-electron model was applied to describe the target structure. Their results were overall in good agreement with the available experiments. It was also reported that, for DCS in He^{2+}-He collisions, including intermediate ionization continua of the two electrons in the exit channel resulted in very good agreement with the experiments.

For the processes of elastic scattering and target excitation, there are no previously available experimental data or theoretical results, to the best of our knowledge. The same is the case for the ionization cross section differential in ejected-electron energy or scattered-projectile angle. However, two approaches were applied to calculate the ionization cross-section differential in ejected-electron angle for ^{3}He^{2+}-He collisions. Bernardi *et al.* [15] presented the CDW-EIS and CTMC results for the ionization SDCS differential in electron angle at the collision energies of 50 and 100 keV/u, together with the experimental data. The underlying theories of the CDW-EIS and CTMC approaches for collisions of fully stripped ions with helium were described in Refs. [24] and [25], respectively. Overall, neither of the theories was able to describe the experimental data sufficiently well. At small ejection angles, the CDW-EIS method underestimated the experimental data for both collision energies.

In this paper, we apply the wave-packet convergent close-coupling (WP-CCC) approach [26,27] to calculate singly differential cross sections in collisions of ^{3}He^{2+} and ^{4}He^{2+} ions with the helium atom. In the wave-packet approach, the continuum of the involved atoms is described by the pseudostates obtained by integrating the corresponding positive-energy wave functions in a certain set of the discretization bins [28]. The WP-CCC approach was successfully applied to study total and differential cross sections for various ion-atom collisions. It was found to be especially suitable in studies of the differential breakup processes as it allows investigating ejected electrons with an arbitrary energy [29–31].

The WP-CCC approach was employed to study collisions involving multielectron targets as well. A single-center version of the approach, applied to collisions of antiprotons and energetic protons with helium, demonstrated a good level of agreement with the available experiments [32]. The two-center WP-CCC approach, which takes the electron-electron correlation into account, was successfully applied to the four-body *p*-He scattering problem to calculate the integrated cross sections for one-electron processes in a wide range of incident energies [26]. Later, it was applied to study singly differential cross sections for electron capture, elastic scattering, target excitation, and ionization [33,34]. It was demonstrated that the WP-CCC approach can accurately describe the singly differential picture of all processes taking place in *p*-He collisions. The WP-CCC method has recently been used to calculate the energy and angular distribution of electrons (i.e., doubly differential cross sections) emitted in *p*-He [35] and *p*-H$_2$ collisions [36] and gave very good agreement with experimental data. Earlier, the method was extended to collisions of fully stripped ions with helium. The total cross sections were calculated for electron capture, elastic scattering, target excitation, and ionization in He^{2+}-He collisions from 10 keV/u to 5 MeV/u, with particular emphasis on the intermediate energies [27]. The obtained results agreed well with the available experimental data for all considered processes.

Here, the two-electron and effective one-electron (E1E) WP-CCC approaches are employed to investigate the singly differential cross sections for one-electron processes in the He^{2+}-He collision system at intermediate projectile energies. This energy range enables us to better understand the importance of coupling between the reaction channels and the electron-electron correlation, which is neglected in the E1E approach. There are experimental [12–15] and theoretical [14,18–23] results available for comparison, but these are mostly for charge transfer. This paper presents comprehensive calculations of the singly differential cross sections for all one-electron processes taking place in He^{2+}-He collisions.

Unless specified otherwise, atomic units (a.u.) are used throughout this paper. Hereafter, we refer to He^{2+} without specifying whether it is the ^{3}He^{2+} or ^{4}He^{2+} isotope when we discuss these projectiles in general or when a particular statement holds for both isotopes.

II. WP-CCC APPROACH

Here we describe application of the two-center WP-CCC approach to the He^{2+}-He system. The approach is based on the total scattering wave function Ψ, which is the solution of the full time-independent Schrödinger equation,

$$(H - E)\Psi = 0, \tag{1}$$

where E is the total energy and H is the full Hamiltonian of the four-body collision system. The total energy can be written in either of the following three forms:

$$E = \epsilon_0 + \frac{k_\alpha^2}{2\mu_T} + \epsilon_\alpha = \epsilon_0 + \frac{k_{1\beta}^2}{2\mu_P} + \epsilon_{1\beta} = \epsilon_0 + \frac{k_{2\beta}^2}{2\mu_P} + \epsilon_{2\beta}, \tag{2}$$

where ϵ_0 is the binding energy of the frozen target electron. The indices α and β denote the full set of quantum numbers representing states in the He^{2+}-He and He^+-He^+ channels, respectively. Channel 1β is the same as channel 2β but with the electron of the residual target and that of the formed (after electron transfer to the projectile) He^+ ion exchanged. Furthermore, $\boldsymbol{k}_\alpha$ is the momentum of the projectile relative to the helium atom in the α channel, μ_T is the reduced mass of this system, ϵ_α is the energy of the pseudostate α, $\boldsymbol{k}_{1\beta}$ ($\boldsymbol{k}_{2\beta}$) is the momentum of the formed He^+ ion relative to the residual helium ion in the 1β (2β) channel, μ_P is the reduced mass, and $\epsilon_{1\beta}$ ($\epsilon_{2\beta}$) is the energy of the He^+ ion in the 1β (2β) channel. We note that $\epsilon_{1\beta} = \epsilon_{2\beta}$.

The full Hamiltonian H can be written as

$$H = K_\sigma + H_{T_1} + H_{T_2} + V_P + V_{12} \tag{3}$$

$$= K_{\rho_1} + H_{P_1} + H_{T_2} + V_1 + V_{12} \tag{4}$$

$$= K_{\rho_2} + H_{P_2} + H_{T_1} + V_2 + V_{12}, \tag{5}$$

where the Hamiltonians of the formed and residual He^+ ions are written as

$$H_{P_i} = -\frac{\nabla_{x_i}^2}{2} - \frac{2}{x_i}, \quad i = 1, 2, \tag{6}$$

$$H_{T_i} = -\frac{\nabla_{r_i}^2}{2} - \frac{2}{r_i}, \quad i = 1, 2, \tag{7}$$

respectively;

$$K_\sigma = -\frac{\nabla_\sigma^2}{2\mu_T}, \quad K_{\rho_i} = -\frac{\nabla_{\rho_i}^2}{2\mu_P}, \; i = 1, 2 \tag{8}$$

are kinetic energy operators and

$$V_P = \frac{4}{R} - \frac{2}{x_1} - \frac{2}{x_2}, \tag{9}$$

$$V_1 = \frac{4}{R} - \frac{2}{r_1} - \frac{2}{x_2}, \tag{10}$$

$$V_2 = \frac{4}{R} - \frac{2}{r_2} - \frac{2}{x_1}, \tag{11}$$

$$V_{12} = \frac{1}{|\boldsymbol{r}_1 - \boldsymbol{r}_2|} \tag{12}$$

are the interaction potentials. Here, the vectors $\boldsymbol{r}_1$ and $\boldsymbol{r}_2$ ($\boldsymbol{x}_1$ and $\boldsymbol{x}_2$), respectively, define the positions of the two electrons relative to the origin (the projectile); $\boldsymbol{\sigma}$ is the position vector

of the projectile relative to the center of mass of the helium atom; and $\boldsymbol{\rho}_1$ ($\boldsymbol{\rho}_2$) is the position vector of the system of the projectile and the first (second) electron relative to the helium ion. See Fig. 1 of Ref. [27] for the Jacobi coordinate system.

We use an impact-parameter representation and a straight-line trajectory approximation. Accordingly, the projectile moves along $\boldsymbol{R} \equiv \boldsymbol{R}(t) = \boldsymbol{b} + \boldsymbol{v}t$ with respect to the target nucleus, fixed at the origin. Here $\boldsymbol{b}$ is the impact parameter, chosen to be perpendicular to $\boldsymbol{v}$, the initial velocity of the projectile, directed along the z axis.

The total scattering wave function is expanded in terms of N target-centered and M projectile-centered pseudostates as

$$\Psi = \sum_{\alpha=1}^{N} F_\alpha(t, \boldsymbol{b}) \psi_\alpha^T(\boldsymbol{r}_1, \boldsymbol{r}_2) e^{i\boldsymbol{k}_\alpha \sigma}$$

$$+ \frac{1}{\sqrt{2}} \sum_{\beta=1}^{M} G_\beta(t, \boldsymbol{b}) \big[\psi_\beta^P(\boldsymbol{x}_1) \psi_0(\boldsymbol{r}_2) e^{i\boldsymbol{k}_{1\beta}\boldsymbol{\rho}_1}$$

$$+ \psi_\beta^P(\boldsymbol{x}_2) \psi_0(\boldsymbol{r}_1) e^{i\boldsymbol{k}_{2\beta}\boldsymbol{\rho}_2} \big], \tag{13}$$

where ψ_α^T and ψ_β^P are the wave functions of the target atom and the hydrogenlike He^+ ion formed after electron capture by the projectile, respectively, and ψ_0 is the ground-state wave function of the residual He^+ ion. Unknown expansion coefficients F_α and G_β represent the transition probability amplitudes.

The pseudostates representing the continuum are constructed using the wave-packet approach [28]. In this approach, the continuum is divided into a number of intervals called discretization bins. Then, the wave packets are obtained by integrating the target (or projectile) continuum wave function over these bins. The positive-energy pseudostates together with the negative-energy eigenstates form a basis used in expansion (13).

We insert the expansion (13) into Eq. (1) and apply the semiclassical approximation. Then, we successively multiply it by the pseudostates and integrate over all variables except for $\boldsymbol{\sigma}$, $\boldsymbol{\rho}_1$, and $\boldsymbol{\rho}_2$ to get the following system of differential equations for the time-dependent coefficients:

$$i\dot{F}_{\alpha'} + i \sum_{\beta=1}^{M} \dot{G}_\beta K_{\alpha'\beta}^T = \sum_{\alpha=1}^{N} F_\alpha D_{\alpha'\alpha}^T + \sum_{\beta=1}^{M} G_\beta Q_{\alpha'\beta}^T,$$

$$i \sum_{\alpha=1}^{N} \dot{F}_\alpha K_{\beta'\alpha}^P + i \sum_{\beta=1}^{M} \dot{G}_\beta L_{\beta'\beta}^P = \sum_{\alpha=1}^{N} F_\alpha Q_{\beta'\alpha}^P + \sum_{\beta=1}^{M} G_\beta D_{\beta'\beta}^P,$$

$$\alpha' = 1, 2, \ldots, N, \quad \beta' = 1, 2, \ldots, M. \tag{14}$$

Note that we start from the exact Schrödinger equation and use a different expansion for the total wave function than other conventional close-coupling approaches, such as the atomic orbital model. However, we arrive at the same set of equations for the expansion coefficients. Moreover, in our approach we do not use the concept of the electron translation factor, which is needed in other close-coupling approaches to adequately represent the rearrangement channels.

Matrix elements for direct scattering read as

$$L_{\beta'\beta}^{\mathrm{P}} = \frac{1}{2}\sum_{i,j=1,2}\langle \boldsymbol{k}_{i\beta'}, \psi_{\beta'}^{\mathrm{P}}, \psi_0 | \psi_\beta^{\mathrm{P}}, \psi_0, \boldsymbol{k}_{j\beta}\rangle, \qquad (15)$$

$$D_{\alpha'\alpha}^{\mathrm{T}} = \langle \boldsymbol{k}_{\alpha'}, \psi_{\alpha'}^{\mathrm{T}} | H_{\mathrm{T}} - E_\alpha^{\mathrm{T}} + V_{\mathrm{P}} | \psi_\alpha^{\mathrm{T}}, \boldsymbol{k}_\alpha\rangle, \qquad (16)$$

$$D_{\beta'\beta}^{\mathrm{P}} = \frac{1}{2}\sum_{i,j=1,2}\langle \boldsymbol{k}_{i\beta'}, \psi_{\beta'}^{\mathrm{P}}, \psi_0 | H_{\mathrm{P}i} - \varepsilon_\beta^{\mathrm{P}} | \psi_\beta^{\mathrm{P}}, \psi_0, \boldsymbol{k}_{j\beta}\rangle$$
$$+ \frac{1}{2}\sum_{i,j=1,2}\langle \boldsymbol{k}_{i\beta'}, \psi_{\beta'}^{\mathrm{P}}, \psi_0 | V_i | \psi_\beta^{\mathrm{P}}, \psi_0, \boldsymbol{k}_{j\beta}\rangle, \qquad (17)$$

and for the rearrangement channels as

$$K_{\beta'\alpha}^{\mathrm{P}} = \frac{1}{\sqrt{2}}\sum_{i=1,2}\langle \boldsymbol{k}_{i\beta'}, \psi_{\beta'}^{\mathrm{P}}, \psi_0 | \psi_\alpha^{\mathrm{T}}, \boldsymbol{k}_\alpha\rangle, \qquad (18)$$

$$K_{\alpha'\beta}^{\mathrm{T}} = \frac{1}{\sqrt{2}}\sum_{i=1,2}\langle \boldsymbol{k}_{\alpha'}, \psi_{\alpha'}^{\mathrm{T}} | \psi_\beta^{\mathrm{P}}, \psi_0, \boldsymbol{k}_{i\beta}\rangle, \qquad (19)$$

$$Q_{\beta'\alpha}^{\mathrm{P}} = \frac{1}{\sqrt{2}}\sum_{i=1,2}\langle \boldsymbol{k}_{i\beta'}, \psi_{\beta'}^{\mathrm{P}}, \psi_0 | H_{\mathrm{T}} - E_\alpha^{\mathrm{T}} + V_{\mathrm{P}} | \psi_\alpha^{\mathrm{T}}, \boldsymbol{k}_\alpha\rangle, \quad (20)$$

$$Q_{\alpha'\beta}^{\mathrm{T}} = \frac{1}{\sqrt{2}}\sum_{i=1,2}\langle \boldsymbol{k}_{\alpha'}, \psi_{\alpha'}^{\mathrm{T}} | H_{\mathrm{P}i} - \varepsilon_\beta^{\mathrm{P}} + V_i | \psi_\beta^{\mathrm{P}}, \psi_0, \boldsymbol{k}_{i\beta}\rangle, \quad (21)$$

where $E_\alpha^{\mathrm{T}} = \epsilon_0 + \epsilon_\alpha$ is the energy of He in channel α, $\varepsilon_\beta^{\mathrm{P}} \equiv \epsilon_{1\beta} = \epsilon_{2\beta}$ is the energy of the formed He$^+$ ion in channel β, and

$$H_{\mathrm{T}} = H_{\mathrm{T}_1} + H_{\mathrm{T}_2} + V_{12}$$

is the Hamiltonian of the helium atom.

The transition probability amplitudes $F_\alpha(+\infty, \boldsymbol{b})$ and $G_\beta(+\infty, \boldsymbol{b})$ are obtained by solving the system of differential equations (14) as $t \to +\infty$, subject to the initial boundary conditions

$$F_\alpha(-\infty, \boldsymbol{b}) = \delta_{\alpha,1s}, \quad \alpha = 1, \dots, N,$$
$$G_\beta(-\infty, \boldsymbol{b}) = 0, \quad \beta = 1, \dots, M. \qquad (22)$$

The differential cross sections are derived from the probability amplitudes. Specifically, singly differential cross sections in the projectile scattering angle for the transition from the initial state i to the final state f are calculated as

$$\frac{d\sigma_{fi}^{\mathrm{DS(EC)}}}{d\Omega} = \frac{\mu_{\mathrm{T}}\mu_f}{(2\pi)^2}\frac{q_f}{q_i}\left|T_{fi}^{\mathrm{DS(EC)}}(\boldsymbol{q}_f, \boldsymbol{q}_i)\right|^2, \qquad (23)$$

where $\Omega = (\theta, \phi)$ is the solid angle of $\boldsymbol{q}_f$ (relative to $\boldsymbol{q}_i$). We set $\boldsymbol{q}_i = \boldsymbol{k}_1$, as the target was assumed to be in its ground state in the initial channel. Depending on the type of scattering, the final momentum is set as either $\boldsymbol{q}_f = \boldsymbol{k}_{\alpha'}$ or $\boldsymbol{q}_f = \boldsymbol{k}_{\beta'}$. Accordingly, the reduced mass μ_f is equal to μ_{T} for the He^{2+}-He channel and to μ_{P} for the He$^+$-He$^+$ channel. The direct-scattering (DS) amplitudes T_{fi}^{DS} and electron-capture (EC) amplitudes T_{fi}^{EC} in momentum space are calculated from the impact-parameter space transition probability amplitudes as

$$T_{fi}^{\mathrm{DS}}(\boldsymbol{q}_f, \boldsymbol{q}_i) = 2\pi i v e^{im\phi_f}\int_0^\infty db\, b[\tilde{F}_f(+\infty, b) - \delta_{fi}]J_m(q_\perp b), \qquad (24)$$

$$T_{fi}^{\mathrm{EC}}(\boldsymbol{q}_f, \boldsymbol{q}_i) = 2\pi i v e^{im\phi_f}\int_0^\infty db\, b\, \tilde{G}_f(+\infty, b)J_m(q_\perp b), \qquad (25)$$

where $q_\perp$ is the magnitude of the perpendicular component of the momentum transfer $\boldsymbol{q} = \boldsymbol{q}_i - \boldsymbol{q}_f$, m is the magnetic quantum number in the final channel, ϕ_f is the azimuthal angle of $\boldsymbol{q}_f$, J_m is the Bessel function of the mth order, $\tilde{F}_f(t, b) = e^{im\phi_b}F_f(t, \boldsymbol{b})$, and $\tilde{G}_f(t, b) = e^{im\phi_b}G_f(t, \boldsymbol{b})$, with ϕ_b being the azimuthal angle of $\boldsymbol{b}$. For more details refer to Ref. [37].

In the WP-CCC method, the ionization amplitude splits into two components: direct ionization (DI) of the target and electron capture into the continuum (ECC) of the projectile [29]. The DI component is written as

$$T^{\mathrm{DI}}(\boldsymbol{\kappa}, \boldsymbol{q}_f, \boldsymbol{q}_i) = \langle \varphi_{\boldsymbol{\kappa}} | \psi_f^{\mathrm{T}}\rangle T_{fi}^{\mathrm{DS}}(\boldsymbol{q}_f, \boldsymbol{q}_i) \qquad (26)$$

and the ECC one is written as

$$T^{\mathrm{ECC}}(\boldsymbol{\varkappa}, \boldsymbol{q}_f, \boldsymbol{q}_i) = \langle \varphi_{\boldsymbol{\varkappa}} | \psi_f^{\mathrm{P}}\rangle T_{fi}^{\mathrm{EC}}(\boldsymbol{q}_f, \boldsymbol{q}_i), \qquad (27)$$

where $\boldsymbol{\kappa}$ ($\boldsymbol{\varkappa}$) is the momentum of the ejected electron relative to the target (projectile) nucleus and $\varphi_{\boldsymbol{\kappa}}$ ($\varphi_{\boldsymbol{\varkappa}}$) is the corresponding true continuum state of helium (the hydrogenlike He$^+$ ion). The DI and ECC amplitudes corresponding to the same ejected-electron momentum should be combined. However, this is not straightforward as they are calculated in different frames of reference. To overcome this problem, we transform the ECC amplitude into the laboratory frame. The electron momentum relative to the projectile $\boldsymbol{\varkappa}$ is written as $\boldsymbol{\kappa} - \boldsymbol{v}$ in the laboratory frame. With that, the fully differential cross section (FDCS) is calculated from the incoherent combination of the DI and ECC components, as

$$\frac{d^3\sigma_{\mathrm{ion}}}{dE_{\mathrm{e}}d\Omega_{\mathrm{e}}d\Omega} = \frac{\mu_{\mathrm{T}}^2}{(2\pi)^5}\frac{q_f\kappa}{q_i}[|T^{\mathrm{DI}}(\boldsymbol{\kappa}, \boldsymbol{q}_f, \boldsymbol{q}_i)|^2 + |T^{\mathrm{ECC}}(\boldsymbol{\kappa} - \boldsymbol{v}, \boldsymbol{q}_f, \boldsymbol{q}_i)|^2], \qquad (28)$$

where $E_{\mathrm{e}} = \kappa^2/2$ is the energy of the ejected electron and Ω_{e} and Ω are the solid angles of the ejected electron and the scattered projectile, respectively. In the laboratory frame, the momentum transfer $\boldsymbol{q}$ is replaced by $\boldsymbol{q} - \boldsymbol{\kappa}$. Therefore, perpendicular component $q_\perp$ is substituted with $(\boldsymbol{q} - \boldsymbol{\kappa})_\perp$ in calculating the integral in Eq. (25).

The coherent and incoherent combinations of the DI and ECC components were investigated by Walters and Whelan [38] and Abdurakhmanov *et al.* [29] in the example of proton-induced ionization of atomic hydrogen. By comparing the coherent and incoherent combinations these authors concluded that the incoherent combination was an acceptable approximation for calculating the differential ionization cross section. It is also consistent with the basic unitarity of the two-center close-coupling formalism. It was also demonstrated that if sufficiently large bases are used in the two-center expansion the incoherent and coherent combinations give practically similar results [29]. This indicates that in the coherent combination the interference term becomes small as the basis size increases. Note that the total ionization cross section is obtained by summing the integrated cross sections for target excitation into the positive-energy pseudostates and electron capture into the continuum of the projectile [27].

The incoherent combination of the components in Eq. (28) is consistent with the definition of the total ionization cross section in the close-coupling formalism. We emphasize that the DI and ECC components of the ionization amplitude are calculated in the two final channels, when the target and projectile are far apart [39]. The DS and EC amplitudes entering Eqs. (26) and (27) are given by the Fourier transform of the impact-parameter space probability amplitudes [see Eqs. (24) and (25)]. These probability amplitudes are calculated using the expansion coefficients in the different final channels in the limit as $t \to +\infty$ where the overlap between the DI and ECC components vanishes. Therefore, it is reasonable to assume that the interference term arising from a coherent combination of T_{fi}^{DS} and T_{fi}^{EC} should approach zero. See Ref. [39] for more discussion.

Integrating the FDCS in Eq. (28) over the corresponding variables, we can obtain three types of the singly differential cross section for ionization. The SDCS in ejected-electron energy is calculated as

$$\frac{d\sigma_{\mathrm{ion}}}{dE_{\mathrm{e}}} = \int \frac{d^3\sigma_{\mathrm{ion}}}{dE_{\mathrm{e}}d\Omega_{\mathrm{e}}d\Omega} d\Omega_{\mathrm{e}}d\Omega, \qquad (29)$$

in the ejected-electron angle as

$$\frac{d\sigma_{\mathrm{ion}}}{d\Omega_{\mathrm{e}}} = \int \frac{d^3\sigma_{\mathrm{ion}}}{dE_{\mathrm{e}}d\Omega_{\mathrm{e}}d\Omega} dE_{\mathrm{e}}d\Omega, \qquad (30)$$

and in the scattered-projectile angle as

$$\frac{d\sigma_{\mathrm{ion}}}{d\Omega} = \int \frac{d^3\sigma_{\mathrm{ion}}}{dE_{\mathrm{e}}d\Omega_{\mathrm{e}}d\Omega} dE_{\mathrm{e}}d\Omega_{\mathrm{e}}. \qquad (31)$$

Total integrated cross sections can be obtained by further integrating the SDCS, which should lead to the same results as the direct summation of the partial cross sections obtained from the probability amplitudes. This fact is used to test the accuracy of the calculations.

In the effective one-electron approach, the helium wave functions are generated using a computational atomic-structure package that is based on the multiconfiguration Hartree-Fock approximation. Using these functions in the expansion of the total scattering wave function, the multielectron Schrödinger equation is reduced to an effective one-electron equation. While this method makes subsequent scattering calculations significantly easier, it neglects the correlation effects between the electrons that become particularly important at lower impact energies. In addition, there is no electron exchange in the He^+-He^+ channel as the residual target ion He^+ is effectively a single particle. More details of the approach are described in Ref. [40], and its application to the helium target is described in Refs. [27,33,34].

Hereafter, we refer to the simplified effective one-electron method as E1E, and we refer to the two-electron method that takes into account the correlation between the target electrons and exchange effects as WP-CCC.

III. RESULTS

A. Details of calculation

In both the two-electron and effective single-electron approaches, the accuracy of the results depends on several factors, such as the helium structure (including the wave functions and energy levels) and the matrix elements used in the differential equation (14). In the two-electron method, the energy levels and the corresponding wave functions of the target were calculated numerically. The obtained energy levels are in very good agreement with the experimental data for all states. In the effective single-electron model, a pseudopotential is generated in such a way that the ground-state energy is the exact experimental value, while for the other states the calculated energy levels agree with the experimental values well. For the hydrogenlike He^+ ion, we used analytic forms of the wave functions and energy levels.

We studied the dependence of the results on the number of discretization bins N_c, the maximum energy of the ejected electron $\epsilon_{\max}$, as well as the maximum principal quantum number of negative-energy states $n_{\max}$ and the maximum angular-momentum quantum number $l_{\max}$ of all the included states. The convergence test was performed by systematically increasing the target and projectile basis sizes, while preserving the accuracy of the employed wave functions for the states. In the impact-parameter approach, the results also depend on the choice of $b_{\max}$, the upper limit for the impact parameter. Unlike for the integrated cross sections, where smaller values of $b_{\max}$ are sufficient to produce reliable results, for the differential cross sections $b_{\max}$ has to be increased up to 30 a.u., depending on the collision energy. The maximum energy of the included bin states, $\epsilon_{\max}$, ranged from 5 to 28 a.u. depending on the incident projectile energy.

For simplicity, in calculations we used an equal number of basis functions for the target and projectile centers. We set $n_{\max} = 8$ and $l_{\max} = 3$, as increasing these values further did not show any significant changes in the final results. The number of the discretization bins ranged from 14 to 22 depending on the projectile energies. The corresponding bases with these parameters include from 318 to 446 functions.

To generate both the two-electron and effective one-electron results, we used recently developed computer codes, which utilize graphics processing units (GPUs). This enabled us to considerably reduce computing time spent on calculations compared with our previous codes, where parallel computations were performed using the central processing units (CPUs). The computation time of the same process with the GPU acceleration is about 200 times less than that of the CPU-based code. For each impact parameter, the computational time was reduced from several hours to 4–5 min, depending on the size of the bases. The speedup in the numerical calculations allowed us to perform large-scale calculations.

B. ³He²⁺-He collisions

In our approach, the integrated cross sections for the $^3He^{2+}$-He and $^4He^{2+}$-He systems are identical when the projectile velocities are equal. However, these two systems should be considered separately for the purpose of calculating the differential cross sections. We first present the E1E and two-electron WP-CCC results for the angular differential cross section for electron capture, elastic scattering, and excitation of the target in $^3He^{2+}$-He collisions. The angular DCSs are calculated using Eq. (23). Then we present all three
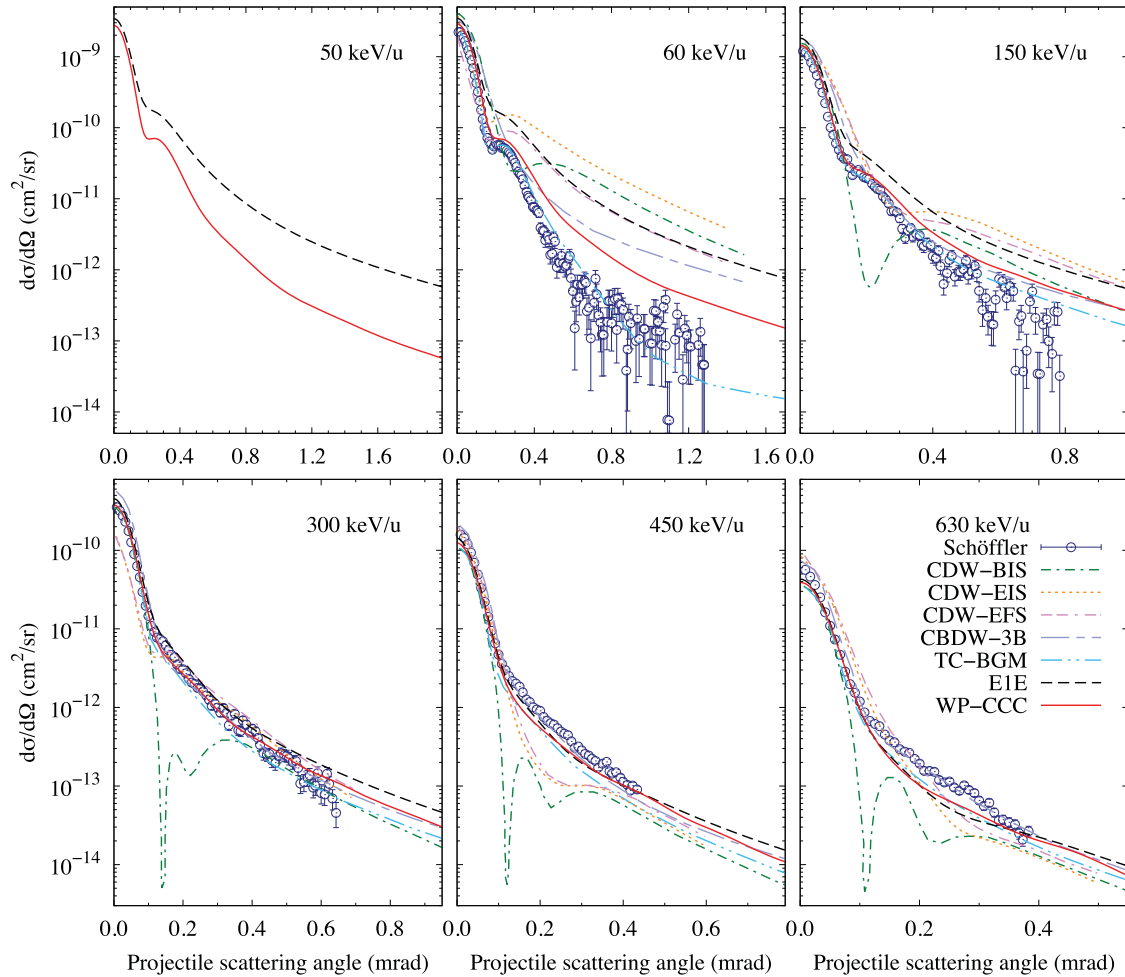
FIG. 1. Angular differential cross section for electron capture into the $1s$ state in $^3\text{He}^{2+}$ -He collisions in the laboratory frame. The present WP-CCC and E1E results are represented by the red solid and black dashed lines, respectively. The experimental data and the CDW-BIS calculations are from Ref. [14], the TC-BGM IEM calculations are from Ref. [17], the CDW-EIS and CDW-EFS calculations are from Ref. [18], and the CBDW-3B calculations are from Ref. [19]. The key shown in the last panel applies to all panels.

types of singly differential cross sections for ionization. These are the cross sections differential in ejected-electron energy, in electron angle, and in scattered-projectile angle. In all figures, the two-electron and effective one-electron WP-CCC results are shown by the red solid and black dashed lines, respectively. All cross sections are given in the laboratory frame.

In Fig. 1, the angular differential cross section is presented for electron capture into the ground state of the hydrogen-like $^3\text{He}^+$ atom at different incident energies. The maximum projectile scattering angle ranges between 0.55 and 2 mrad, depending on the projectile energy. Our calculations are compared with the experimental data of Schöffler *et al.* [14]. It was noticed that for the projectile energy of 450 keV/u the experimental data points above 0.43 mrad got affected by the reduced solid angle for large transverse momenta. Therefore, here only the data below 0.43 mrad are shown. Also included in Fig. 1 are other theoretical results: the CDW-BIS calculations of Schöffler *et al.* [14], the TC-BGM IEM calculations of Zapukhlyak and Kirchner [17], the CDW-EIS and CDW-EFS calculations of Velayati *et al.* [18], and the CBDW-3B calculations of Ghanbari-Adivi and Ghavaminia [19]. Overall we can observe noticeable discrepancies between the theories,

especially at small collision energies. In Ref. [14], in line with the experimental data, the theoretical results based on the CDW-BIS approach are also given. At all considered incident energies, the CDW-BIS results are in good agreement with the experiment in a narrow region in the forward direction. However, the approach fails to describe the experimental data at larger angles. The approach also shows some dips as the scattering angle increases, which is not observed in the experiment.

At 50 keV/u, where no experimental data are available, the WP-CCC calculations show that the cross section peaks in the forward direction and displays a shoulder structure around 0.3 mrad. The shoulder structure is also observed at collision energies up to 150 keV/u, and it washes out at higher energies. The experimental data and other theoretical results are available at projectile energy 60 keV/u and above. The most challenging collision energy for the theoretical approaches appears to be 60 keV/u, where considerable deviations can be observed between the theories and the experiment. Discrepancies are especially noticeable at larger scattering angles, where practically all the theoretical results fail to describe the experimental data, except for the
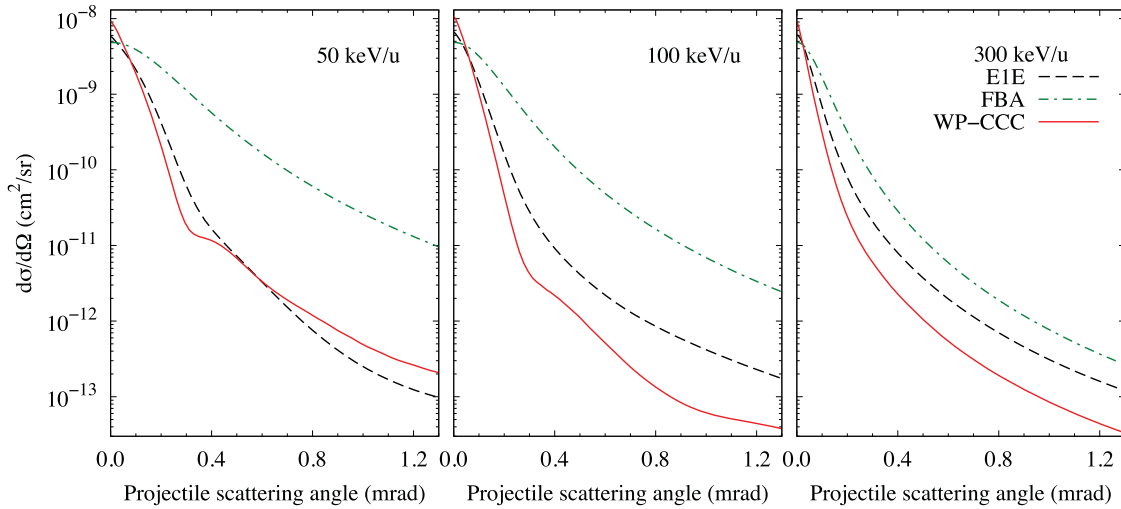
FIG. 2. Angular differential cross section for elastic scattering in $^3He^{2+}$ -He collisions in the laboratory frame. The present WP-CCC and E1E results are represented by the red solid and black dashed lines, respectively. The present FBA results obtained within the E1E method are also depicted. The key shown in the last panel applies to all panels.

TC-BGM IEM calculations that agree with the experiment very well. We note that the present WP-CCC and the TC-BGM results reproduce the shoulder seen in the experiment very well. Our calculations are in good agreement with the experiment below 0.3 mrad, but overestimate the data at larger scattering angles. A similar behavior of the WP-CCC cross sections with respect to the experimental data can be seen at 150 keV/u, but with relatively smaller deviation at larger scattering angles. At 300 keV/u, the WP-CCC results are in very good agreement with the experiment across the entire scattering angle range. In fact, all theories except for CDW-BIS, CDW-EIS, and CBDW-3B are in very good agreement with the experimental data. The WP-CCC results describe the experimental data generally well at 450 and 630 keV/u too. At 630 keV/u they slightly underestimate the data in the 0.15–0.3-mrad region. Here, all methods including the TC-BGM IEM results also underestimate the experiment. The present E1E calculations exceed the two-electron WP-CCC ones and, where available, the experiment below 150 keV/u. This highlights the importance of the electron-electron correlation in the electron-transfer processes at relatively small collision energies. Similar conclusions were drawn for the total electron-capture cross sections in Ref. [27]. The shoulder structure mentioned above is also poorly described. One can conclude that a correlated two-electron description of the target is needed in order to reveal this feature. Starting from 300 keV/u, the E1E and WP-CCC results agree with each other reasonably well.

Figures 2 and 3 present the WP-CCC results for the angular differential cross section for elastic scattering and excitation into all excited states of the target, respectively. We note that the calculations are performed at all six projectile energies shown in Fig. 1; however, hereafter we give the results only at three energies. For both processes, the two-electron WP-CCC results reveal a shoulder structure at 50 keV/u, somewhat similar to that observed for electron capture. But at larger energies no shoulder is seen. Another interesting observation is that, for elastic scattering, the magnitude of the cross section in the forward direction remains almost the same at all projectile energies considered here. However, the cross section falls off as a function of scattering angle faster with increasing projectile energy [27]. The differential excitation cross section peaks in the forward direction and exponentially decreases as the scattering angle increases. There are no previously available experimental or other theoretical results for elastic scattering and excitation. Therefore, we compare only the E1E and two-electron WP-CCC results. For elastic scattering, at all collision energies, the two-electron results are larger near the forward direction, but then drop below the E1E results. At 100 and 300 keV/u, the deviation between the E1E and two-electron WP-CCC results becomes larger as the scattering angle increases. In addition, we include the results for elastic scattering obtained using the FBA within the E1E method. We can see that at the considered energies the FBA results are sufficiently close to the full calculations in the forward direction. However, they noticeably deviate from the latter as the scattering angle increases. At 300 keV/u, the deviation is smaller than that at 50 and 100 keV/u, as expected. For excitation, at all projectile energies, the agreement between the results is very good at smaller scattering angles but the results slightly deviate as the scattering angle increases. Overall, the agreement between the results for excitation is better than that for elastic scattering. This can be explained by the different target descriptions used in these two approaches. The elastic scattering is particularly sensitive to the ground state of the helium atom, however the active electron becomes less sensitive to the target structure as it transitions to the excited states.

In the next three figures, we present the singly differential cross sections for ionization. The ionization cross section differential in ejected-electron energy is presented in Fig. 4. This SDCS is calculated using Eq. (29). The DI and ECC components of the two-electron WP-CCC results are also shown in the figure to highlight their contribution. It is seen that at all collision energies the direct ionization component peaks when very slow electrons are ejected. At the projectile
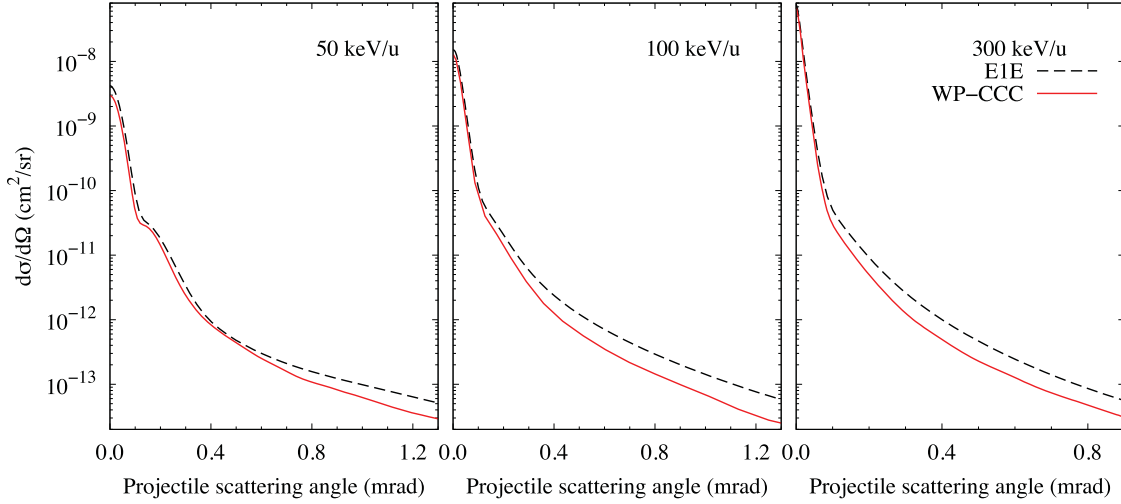
FIG. 3. Angular differential cross section for excitation in $^3He^{2+}$ -He collisions in the laboratory frame. The present WP-CCC and E1E results are represented by the red solid and black dashed lines, respectively. The key shown in the last panel applies to all panels.

energy of 50 keV/u, the cross section has a peak around 20-eV emission energy, where ECC contributes significantly more than DI. At 100 keV/u, the ECC peak is not dominant enough to produce a peak in the ionization cross section but shows up as a shoulder. The shoulder disappears at 300 keV/u due to diminishing significance of the ECC component, where the cross section falls steadily as the ejection energy increases. We also note that the E1E results, presented at all projectile energies, are in very good agreement with the two-electron WP-CCC ones.

Figure 5 presents the ionization cross-section differential in the ejected-electron angle. The cross section is calculated using Eq. (30). At the projectile energies of 50 and 100 keV/u, our results are compared with the experimental data, the CTMC and CDW-EIS calculations by Bernardi *et al.* [15]. The WP-CCC results slightly underestimate the available experimental points at 50 keV/u. However, they are in

excellent agreement with the experiment at 100 keV/u. In comparison with other theoretical calculations, we can see that the WP-CCC results mostly lie between the CDW-EIS and CTMC calculations at both collision energies. The DI and ECC components of the two-electron WP-CCC results are also shown. The DI and ECC components reveal that at 50 and 100 keV/u the ionization cross sections are mostly due to ECC at small ejection angles and DI at large angles including the backward ejection. We also note that at 300 keV/u DI has a dominant contribution in the ionization SDCS at all ejection angles except for a very narrow cone near the forward direction. At all collision energies, the E1E and two-electron WP-CCC results are in overall good agreement. At 50 keV/u, the one-electron approach produces a shallow peak in the backward direction. This may be because of the inability of the E1E approach to properly describe the back-
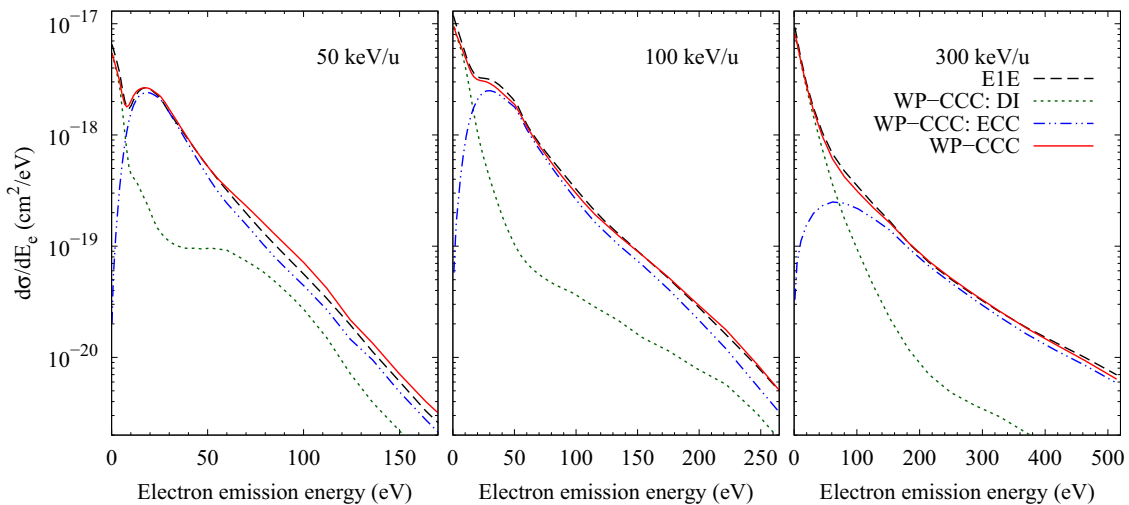

FIG. 4. Singly differential cross section for ionization in $^3He^{2+}$ -He collisions as a function of ejected-electron energy. The present WP-CCC and E1E results are represented by the red solid and black dashed lines, respectively. The key shown in the last panel applies to all panels.
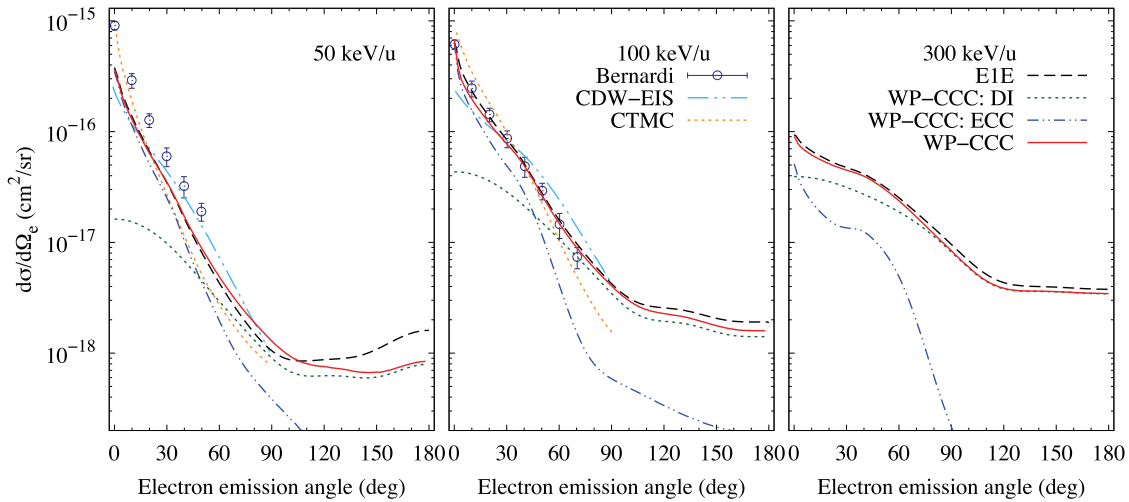
FIG. 5. Singly differential cross section for ionization in ^{3}He^{2+} -He collisions as a function of ejected-electron angle. The present WP-CCC and E1E results are represented by the red solid and black dashed lines, respectively. Experimental data and CDW-EIS and CTMC calculations are by Bernardi *et al.* [15]. The keys shown in the last two panels apply to all panels.

ward electron ejection, when the collision energy is relatively 6 small.

Figure 6 shows the E1E and two-electron WP-CCC results for the ionization cross section differential in the projectile scattering angle. Both methods produce exponentially decreasing but otherwise featureless cross sections at all projectile energies. We note, however, that a shoulder feature is seen at 50 keV/u reminiscent of that seen in our results for the differential cross section for excitation. In ion-atom collisions, the target electron is less likely to change the direction of the incoming projectile to large angles. Therefore, in Figs. 2, 3, and 6, the corresponding cross sections fall off sharply as the projectile scattering angle increases. Large-angle scattering happens due to the interaction between the projectile and the target nucleus, especially for slow projectiles. This indicates that at small projectile scattering angles the angular

differential cross sections are mostly due to electron-projectile interaction, while at larger angles heavy-particle interaction becomes more important. The change in the character of the interaction as the scattering angle increases must be the physical reason behind the shoulders observed in these figures. At 50 and 100 keV/u, ECC is the dominant mechanism throughout the whole scattering-angle region of interest, while at 300 keV/u DI becomes dominant (the DI and ECC components are not shown in the figure since in all cases the dominant component is little different from the total). As has been observed for other types of SDCS for ionization, there is very good agreement between the present E1E and two-electron approaches. This reveals that within the wave-packet approach the E1E model describes the continuum of the helium atom sufficiently well. It allows us to conclude that all three types of the singly differential cross sections for ioniza-
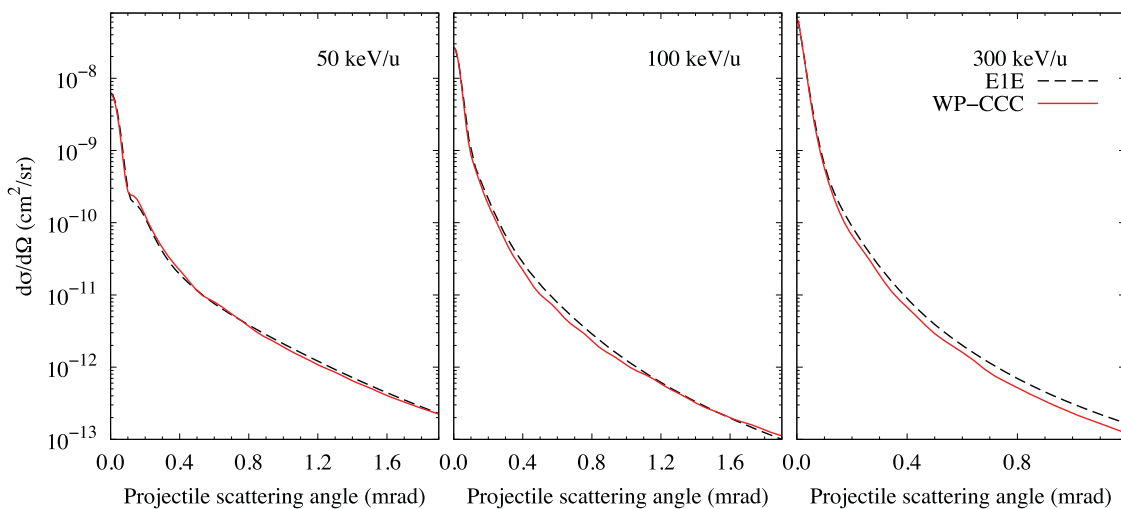

FIG. 6. Singly differential cross section for ionization in ^{3}He^{2+} -He collisions in scattered-projectile angle in the laboratory frame. The present WP-CCC and E1E results are represented by the red solid and black dashed lines, respectively. The key shown in the last panel applies to all panels.
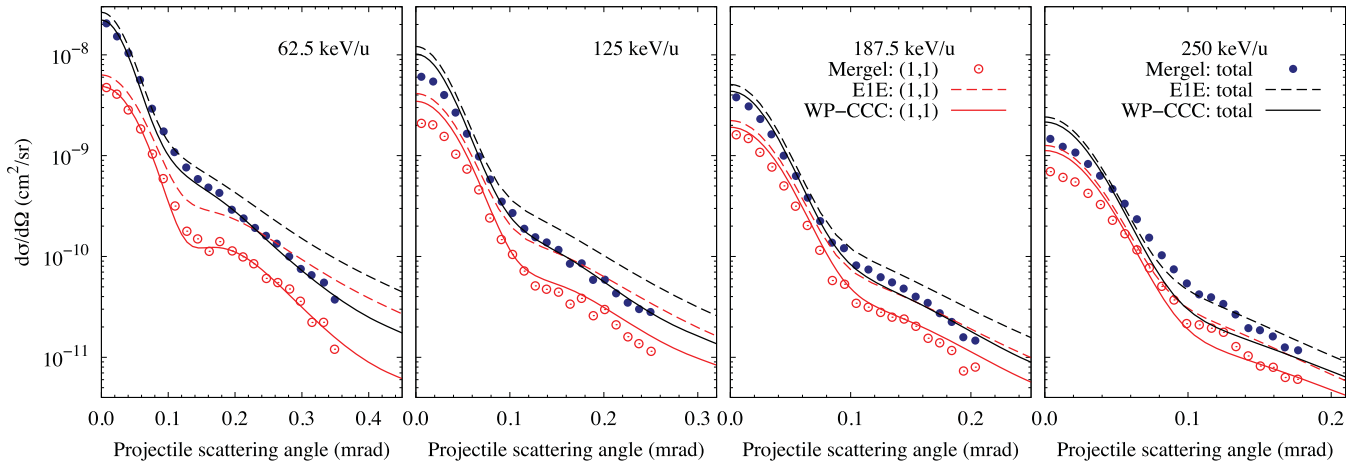
FIG. 7. Angular differential cross sections for ground-state and total electron capture in ^{4}He^{2+}-He collisions in the laboratory frame. The experimental data are from Mergel *et al.* [12,13]. The present WP-CCC and E1E results are given as the solid and dashed lines, respectively. The keys shown in the last two panels apply to all panels.

tion can be described by the effective single-electron model, a much simpler alternative to the two-electron approach.

C. ^{4}He^{2+}-He collisions

In this section, we discuss the angular differential cross sections for ground-state and total electron capture in ^{4}He^{2+}-He collisions at the incident energies of 62.5, 125, 187.5, and 250 keV/u. Slightly different collision energies are chosen for this system to be able to compare with the available experimental data. Theoretical treatment of this collision system is similar to that of ^{3}He^{2+}-He collisions. However, as we mentioned before, it is experimentally challenging due to its symmetry. Especially, for electron-capture processes, when both the formed and the residual ions are ^{4}He$^+$, separation of the reaction products becomes a difficult task. Here, we follow the traditional notation (n, n') to describe the reaction ^{4}He^{2+}-He$(1s^2) \rightarrow$ ^{4}He$^+(n) - $ ^{4}He$^+(n')$, where the first electron is captured into the nth state of the projectile, and the second electron is excited into the n'th state of the residual ion (transfer excitation). Experiments cannot distinguish the (n, n') and (n', n) processes. Therefore, conventionally, for this symmetric collision system the cross sections are presented for the reactions $(n, n') + (n', n)$. Mergel *et al.* [12,13] measured the differential cross sections for the reaction $(1,1)$ and for total transfer excitation, which is the combination of all possible reactions $(n, n') + (n', n)$.

In Fig. 7, we present the angular differential cross section for electron capture into the ground state, referred to as $(1,1)$, and compare with the corresponding experimental data of Mergel *et al.* [12,13]. In addition, we compare our results for total electron capture, which is the sum of partial electron-capture cross sections into all bound states of the projectile, with the data for total transfer excitation. We note that in our approach the target is treated using the frozen-core approximation, where one of the electrons stays in its ground state throughout the collision. Therefore, it does not account for transfer-excitation processes. At 62.5 keV/u, we observe excellent qualitative and quantitative agreement be-

tween the WP-CCC calculations and the experiment for the ground-state electron capture. The oscillatory structure of the cross section seen in the experimental results is accurately reproduced in our calculations. Our total electron-capture cross sections are also in excellent agreement with the experimental data for total transfer excitation. This indicates the dominance of the $(n, 1)$ reactions in transfer-excitation processes. At 125 keV/u, the two-electron WP-CCC results are in good agreement with the experimental data except for small scattering angles where they slightly overestimate the data. Agreement between our results and the experiment is very good again at 187.5 keV/u, however it is slightly worse at 250 keV/u. As in the case of ^{3}He^{2+}-He collisions, the E1E results slightly overestimate the WP-CCC ones, especially at large scattering angles for both ground-state and total electron capture. Finally, we have also calculated the angular differential elastic-scattering and excitation cross section, and all three types of the singly differential ionization cross sections. However, they are found to be practically the same as the corresponding results for ^{3}He^{2+}-He collisions (when calculated at the same projectile velocity). Therefore, they are not presented. One can conclude that the symmetry property mentioned above must be less relevant to these channels.

IV. SUMMARY AND CONCLUSIONS

To summarize, the two-electron and effective one-electron wave-packet convergent close-coupling approaches have been applied to study the singly differential cross sections for all one-electron processes taking place in ^{3}He^{2+}-He and ^{4}He^{2+}-He collisions. In the two-electron approach, the correlation between the target electrons and electron-exchange effects between the reaction fragments were fully taken into account. The effective single-electron method does not account for these effects, but it allowed us to study the collisional system in a more efficient way, in terms of numerical calculations, and provided a good test for the two-electron WP-CCC results, especially for the processes where no experimental results were found for comparison. In both approaches, the continuum for the target and projectile atoms

was described using the wave-packet pseudostates obtained by integrating the corresponding continuum function in a certain set of discretization bins. The singly differential cross sections were calculated for the ground-state and total electron capture, elastic scattering, excitation, as well as ionization of the target for both collision systems. We considered an intermediate incident energy range of 50–630 keV/u, where one-electron processes are expected to be dominant.

For electron capture into the ground state in ^{3}He^{2+}-He collisions, the WP-CCC results showed overall good agreement with the experimental data of Schöffler *et al.* [14], where available. At 60 and 150 keV/u, we observed some discrepancies at larger angles, where the theoretical calculations showed considerable deviations. For elastic scattering and excitation, no experiments are available for comparison. The WP-CCC results for both processes showed that the angular DCS peaks in the forward direction and steadily falls as the projectile scattering angle increases. We also observed that the two-electron WP-CCC cross sections possess a shoulder structure at smaller collision energies. This feature was found to be common for all angular differential cross sections. The WP-CCC results were presented for all types of SDCS for ionization. The calculated SDCS differential in ejected-electron angle described the experimental data of Bernardi *et al.* [15] very well at 100 keV/u, but slightly underestimated it at 50 keV/u. The DI and ECC components of the SDCS were also presented. For the SDCS differential in ejected-electron energy, this explained the reason of the second peak of the cross section at 50 keV/u, and a shoulder at 100 keV/u, to be due to the ECC peak.

For ^{4}He^{2+}-He collisions, the experimental data were presented by Mergel *et al.* [12,13] for angular differential electron capture at collision energies from 62.5 to 250 keV/u. The results given in this paper represent the theoretical analysis of the aforementioned experimental data. For electron capture into the ground state, we observed excellent agreement between the WP-CCC results and the data at 62.5 and 187.5 keV/u. However, at 125 and 250 keV/u, WP-CCC results slightly overestimated the data at small scattering angles. A similar situation was observed between the WP-CCC results for total electron capture and the experimental data for total transfer excitation. We also observed that the cross sections for the other processes taking place in ^{4}He^{2+}-He collisions are very similar to those for the ^{3}He^{2+}-He system. They did not show any new features either quantitatively or qualitatively. Therefore, we did not present these results. However, they are available from the authors by request. It is concluded that the symmetry property of the ^{4}He^{2+}-He collision system is less relevant to the elastic-scattering, excitation, and ionization channels.

We emphasize that the scattering amplitudes calculated in this paper depend only on the momentum transfer. Therefore, for a given value of the momentum transfer, the amplitudes for the two collision systems are identical. The kinematic factors in the definitions of the cross sections are slightly different due to the difference in the masses. Accordingly, at each collision energy, the differential cross sections presented in this paper for one particular system can be scaled as functions of the transverse momentum transfer and used for the other system after the correction for the difference in the kinematic factor.

This applies to all the results except for the total transfer-excitation ones shown in Fig. 7. This remark may indicate that plotting the angular differential cross sections as functions of the transverse momentum transfer would make the aforementioned generalization simpler. However, generally speaking, it is not an optimal way of presenting the results. The main reason why we present our results as functions of the scattering angle is the following. When the differential cross sections are plotted as functions of the perpendicular component of the momentum transfer, the most important (from a physics point of view) region of low momentum transfer, where scattering mostly happens, gets suppressed due to the presence of $\sin\theta$. Instead, the focus shifts to the regions that are less important (meaning the regions with much less flux). The disadvantage of presenting the differential cross sections as functions of the momentum transfer becomes particularly evident when one considers the fully and doubly differential cross sections in the forward direction. Therefore, here in this paper and in our previous papers, we use the scattering angle as the main variable.

In general, it is concluded that the two-electron WP-CCC approach is able to reproduce the general differential picture of both the ^{3}He^{2+}-He and ^{4}He^{2+}-He collisional systems in terms of the angular differential cross sections for electron capture at all considered collision energies. However, the effective one-electron method is found to produce accurate differential electron-capture cross sections only at sufficiently larger projectile energies. This shows the importance of properly accounting for the electron-electron correlations in the target treatment and electron-exchange effects between the reaction products in the electron-transfer channels in studying electron-capture processes. The present approaches were also found to accurately describe the experimental data for the SDCS for ionization as a function of the ejected-electron angle, where available. For excitation and other types of SDCS for ionization, there are no experimental or theoretical results for comparison. However, the agreement observed between the results of the effective one-electron and two-electron WP-CCC methods gives us some confidence about the accuracy of the approaches in describing those processes as well. Experimental and other theoretical studies would be desirable to verify these results.

We plan to further develop the WP-CCC approach to investigate two-electron processes, such as transfer excitation and transfer ionization in ion collisions with He [41,42], where agreement between theory and experiment remains unsatisfactory. We also plan to revisit the widely discussed problem of kinematically complete single ionization of helium by C^{6+} ions [43] using the two-center WP-CCC method. The single-center quantum-mechanical version of the convergent close-coupling method was applied to the problem [44]; however, the results did not agree with the experiment.

---

[1] M. Alessi, S. Otranto, and P. Focke, Phys. Rev. A **83**, 014701 (2011).

[2] M. E. Rudd, R. D. DuBois, L. H. Toburen, C. A. Ratcliffe, and T. V. Goffe, Phys. Rev. A **28**, 3244 (1983).

[3] H. Knudsen, L. H. Andersen, P. Hvelplund, G. Astner, H. Cederquist, H. Danared, L. Liljeby, and K. G. Rensfelt, J. Phys. B **17**, 3545 (1984).

[4] M. E. Rudd, T. V. Goffe, and A. Itoh, Phys. Rev. A **32**, 2128 (1985).

[5] N. V. de Castro Faria, F. L. Freire, and A. G. de Pinho, Phys. Rev. A **37**, 280 (1988).

[6] M. B. Shah and H. B. Gilbody, J. Phys. B **18**, 899 (1985).

[7] M. B. Shah, P. McCallion, and H. B. Gilbody, J. Phys. B **22**, 3037 (1989).

[8] K. M. Dunseath and D. S. F. Crothers, J. Phys. B **24**, 5003 (1991).

[9] P. N. Abufager, A. E. Martínez, R. D. Rivarola, and P. D. Fainstein, J. Phys. B **37**, 817 (2004).

[10] I. Mančev, N. Milojević, and Dž. Belkić, At. Data Nucl. Data Tables **102**, 6 (2015).

[11] D. Delibašić, N. Milojević, I. Mančev, and D. Belkić, At. Data Nucl. Data Tables **148**, 101530 (2022).

[12] V. Mergel, R. Dörner, J. Ullrich, O. Jagutzki, S. Lencinas, S. Nüttgens, L. Spielberger, M. Unverzagt, C. L. Cocke, R. E. Olson, M. Schulz, U. Buck, E. Zanger, W. Theisinger, M. Isser, S. Geis, and H. Schmidt-Böcking, Phys. Rev. Lett. **74**, 2200 (1995).

[13] V. Mergel, R. Dörner, J. Ullrich, O. Jagutzki, S. Lencinas, S. Nüttgens, L. Spielberger, M. Unverzagt, C. Cocke, R. Olson, M. Schulz, U. Buck, and H. Schmidt-Böcking, Nucl. Instrum. Methods Phys. Res., Sect. B **98**, 593 (1995).

[14] M. S. Schöffler, J. Titze, L. P. H. Schmidt, T. Jahnke, N. Neumann, O. Jagutzki, H. Schmidt-Böcking, R. Dörner, and I. Mančev, Phys. Rev. A **79**, 064701 (2009).

[15] G. C. Bernardi, S. Suárez, P. D. Fainstein, C. R. Garibotti, W. Meckbach, and P. Focke, Phys. Rev. A **40**, 6863 (1989).

[16] C. Hill, Dipti, K. Heinola, A. Dubois, N. Sisourat, A. Taoutioui, H. Agueny, K. Tőkési, I. Ziaeian, C. Illescas, A. Jorge, L. Méndez, A. Kadyrov, N. Antonio, A. Kotian, T. Kirchner, A. Leung, J. Ko, J. Lee, O. Marchuk, M. O'Mullane, E. Litherland-Smith, G. Pokol, O. Asztalos, P. Balazs, Y. Wu, C. Jia, L. Liu, and J. Wang, Nucl. Fusion **63**, 125001 (2023).

[17] M. Zapukhlyak and T. Kirchner, Phys. Rev. A **80**, 062705 (2009).

[18] A. Velayati, E. Ghanbari-Adivi, and O. Ghorbani, J. Phys. B **51**, 185201 (2018).

[19] E. Ghanbari-Adivi and H. Ghavaminia, J. Phys. B **45**, 235202 (2012).

[20] E. Ghanbari-Adivi and H. Ghavaminia, Few-Body Syst. **55**, 1109 (2014).

[21] S. Jana and M. Purkait, Indian J. Phys. **88**, 343 (2014).

[22] S. Jana, C. R. Mandal, and M. Purkait, J. Phys. B **48**, 045203 (2015).

[23] S. Samaddar, S. Halder, A. Mondal, C. R. Mandal, M. Purkait, and T. K. Das, J. Phys. B **50**, 065202 (2017).

[24] P. D. Fainstein, V. H. Ponce, and R. D. Rivarola, Phys. Rev. A **36**, 3639 (1987).

[25] R. E. Olson, T. J. Gay, H. G. Berry, E. B. Hale, and V. D. Irby, Phys. Rev. Lett. **59**, 36 (1987).

[26] S. U. Alladustov, I. B. Abdurakhmanov, A. S. Kadyrov, I. Bray, and K. Bartschat, Phys. Rev. A **99**, 052706 (2019).

[27] S. U. Alladustov, C. T. Plowman, I. B. Abdurakhmanov, I. Bray, and A. S. Kadyrov, Phys. Rev. A **106**, 062819 (2022).

[28] I. B. Abdurakhmanov, A. S. Kadyrov, and I. Bray, Phys. Rev. A **94**, 022703 (2016).

[29] I. B. Abdurakhmanov, J. J. Bailey, A. S. Kadyrov, and I. Bray, Phys. Rev. A **97**, 032707 (2018).

[30] I. B. Abdurakhmanov, K. Massen-Hane, S. U. Alladustov, J. J. Bailey, A. S. Kadyrov, and I. Bray, Phys. Rev. A **98**, 062710 (2018).

[31] C. T. Plowman, I. B. Abdurakhmanov, I. Bray, and A. S. Kadyrov, Eur. Phys. J. D **76**, 129 (2022).

[32] I. B. Abdurakhmanov, A. S. Kadyrov, I. Bray, and K. Bartschat, Phys. Rev. A **96**, 022702 (2017).

[33] K. H. Spicer, C. T. Plowman, I. B. Abdurakhmanov, A. S. Kadyrov, I. Bray, and S. U. Alladustov, Phys. Rev. A **104**, 032818 (2021).

[34] K. H. Spicer, C. T. Plowman, I. B. Abdurakhmanov, S. U. Alladustov, I. Bray, and A. S. Kadyrov, Phys. Rev. A **104**, 052815 (2021).

[35] K. H. Spicer, C. T. Plowman, S. U. Alladustov, I. B. Abdurakhmanov, I. Bray, and A. S. Kadyrov, Eur. Phys. J. D **77**, 131 (2023).

[36] C. T. Plowman, I. B. Abdurakhmanov, I. Bray, and A. S. Kadyrov, Phys. Rev. A **107**, 032824 (2023).

[37] B. H. Bransden and M. R. C. McDowell, *Charge Exchange and the Theory of Ion-Atom Collisions* (Clarendon, Oxford, 1992).

[38] H. R. J. Walters and C. T. Whelan, Phys. Rev. A **92**, 062712 (2015).

[39] C. T. Plowman, K. H. Spicer, and A. S. Kadyrov, Atoms **11**, 112 (2023).

[40] I. B. Abdurakhmanov, C. T. Plowman, K. H. Spicer, I. Bray, and A. S. Kadyrov, Phys. Rev. A **104**, 042820 (2021).

[41] M. S. Schöffler, J. N. Titze, L. P. H. Schmidt, T. Jahnke, O. Jagutzki, H. Schmidt-Böcking, and R. Dörner, Phys. Rev. A **80**, 042702 (2009).

[42] M. S. Schöffler, H.-K. Kim, O. Chuluunbaatar, S. Houamer, A. G. Galstyan, J. N. Titze, T. Jahnke, L. P. H. Schmidt, H. Schmidt-Böcking, R. Dörner, Y. V. Popov, and A. A. Bulychev, Phys. Rev. A **89**, 032707 (2014).

[43] M. Schulz, R. Moshammer, D. Fischer, H. Kollmus, D. H. Madison, S. Jones, and J. Ullrich, Nature (London) **422**, 48 (2003).

[44] I. B. Abdurakhmanov, I. Bray, D. V. Fursa, A. S. Kadyrov, and A. T. Stelbovics, Phys. Rev. A **86**, 034701 (2012).